JSR Publications

Available Online

J. Sci. Res. **16** (1), 289-299 (2024)

JOURNAL OF SCIENTIFIC RESEARCH

www.banglajol.info/index.php/JSR

Investigation of the Photocatalytic Activity of Carbon Doped TiO_2 for Photodegration of Methylene Blue

J. S. Bharambe[1*], P. Borgaonkar[2], V. B. Pujari[3]

[1]ICLES' Motilal Jhunjhunwala College of Arts Science and Commerce, Vashi, Navi Mumbai, India

[2]Vikas college of Arts, Science and Commerce, Vikhroli, Mumbai, India

[3]Karmaveer Bhaurao Patil College, Vashi, Navi Mumbai, India

Received 26 April 2023, accepted in final revised form 27 October 2023

Abstract

Nanoparticles of pure TiO_2 and carbon doped TiO_2 (at various concentrations 1, 2, 3 and 4 %) were synthesised by Sol gel method using titanium butoxide and glucose as a precursors for Titanium dioxide and carbon respectively. The samples were calcinated at 500 °C. Photocatalytic activity of the samples was tested for photodegradation of methylene blue dye. Morphological and elemental analysis of the samples were carried out using a scanning electron microscope (SEM), energy dispersive X-ray spectroscopy (EDAX), X-ray diffraction and micro-raman spectroscopy while for optical characterization UV-Vis diffuse reflectance spectra were employed. Results of all samples indicated crystallite growth in a tetragonal structure with the variation in crystallite size in the range 9 nm to 12.6 nm with increase in the concentration of dopant in TiO_2. Diffused reflectance spectroscopy (DRS) analysis indicated that the band gap of all doped TiO_2 nanoparticles is lesser than that of the pure TiO_2 whereas 4C-TiO_2 showed smallest band gap (2.98 eV). The maximum photocatalytic activity was observed with 4C-TiO_2 among all the samples.

Keywords: C-doped TiO_2; Sol-Gel method; Morphological; Photocatalytic degradation; Methylene Blue.

doi: http://dx.doi.org/10.3329/jsr.v16i1.65770 J. Sci. Res. **16** (1), 289-299 (2024)

1. Introduction

Environmental pollution has increased the need for cutting-edge research into methods for effectively removing hazardous chemicals released into the environment. If these toxins are not eliminated, it will have a negative impact on both human health and the ecosystem [1]. A number of techniques have been proposed to remove contaminants from aqueous solutions, including flocculation, reverse osmosis, coagulation, adsorption, and ultrafiltration on solid surfaces. To handle the trash and sludge generated by these methods, different treatment techniques must be employed [2,3]. Recent technological advancements have led to a rise in the popularity for photocatalytic wastewater degradation due to its simple and environmentally beneficial processes. The low cost,

* *Corresponding author*: jyotibharambe@yahoo.com

distinctive photoelectric characteristics, chemical stability, and environmental and human safety of TiO_2 have made it a popular semiconductor photocatalyst for wastewater treatment [4]. TiO_2 has a wide bandgap (3.2 eV), which inhibits its ability to be effectively activated by light besides UV radiation. As a result, only a very small portion (3-5 %) of the light from the solar spectrum is utilized during photocatalysis [5]. TiO_2 photocatalyst needs to be sensitized to absorb visible light in order to utilize a significant portion of the solar spectrum effectively. A lot of work has been put towards expanding the photocatalyst's photoresponse into the visible spectrum, which comprises about 55% of solar light [6]. Another challenge is the rapid rate of recombination of the photogenerated electron-hole pairs, which can be reduced by incorporating charge traps for either both or individual charges in order to slow down the rate of recombination [7]. To deal with this issue, various kinds of techniques have been used, namely semiconductor coupling, surface modification employing organic materials, non-metal and/or metal doping in TiO_2, transition metal deposition, and photosensitization of dye on the surface of TiO_2 [8,9]. Doping is a frequently employed technique during which the TiO_2 lattice is introduced with either donor or acceptor impurities, directly reducing the effective bandgap. The doped ions contribute additional energy levels, trapping more electrons and holes at the surface and causing a shift in the absorption edge towards the visible region of the spectrum [10,11]. Zinc (Zn), nickel (Ni), cobalt (Co) [12,13] manganese (Mn) [12], barium (Ba), palladium (Pd) [14,15], iron (Fe) [16], copper (Cu), silver (Ag) [15], chromium (Cr) [15,17] metals when doped in TiO_2 exhibited a red shift in the absorption edge, enhancing the photocatalytic activity of TiO_2. Metal-doped TiO_2 has, however, been reported to have a number of adverse effects, including thermodynamic instability, a boost in electron-hole recombination centers, the insolubility of the dopants, and fluctuations in the diffusion length of the charge carriers [18].

A number of studies have demonstrated that nonmetal doping has great potential for generating visible light-responsive photocatalysts. Non-metal doped TiO_2 creates an additional energy level above the edge of the valence band of TiO_2 [19]. Incorporating different non-metal dopants like carbon (C) [20], sulphur (S) [21], nitrogen (N) [22-25], phosphorus and fluorine (F) [17] into TiO_2 can improve its morphology and photocatalytic efficacy. The photoelectrochemical and photocatalytic properties of non-metal doped TiO_2 have been enhanced as the band gap of TiO_2 narrows, the specific surface area and anatase phase percentage rise, and the spectra of nanodoped TiO_2 indicated a red shift towards the visible region [19]. Photocatalysts can absorb visible light as the band gap narrows due to non-metal-doped TiO_2 creating new impurity energy levels above the valence band.

Carbon doping of TiO_2 is thought to be the most promising approach among nonmetal doping as it yields the highest redshift of the valence band edge [4,26,27]. The effect of carbon content on the photocatalytic performance of carbon doped TiO_2 for the photodegradation of methylene blue is explored in this experiment where pure and Carbon doped TiO_2 are made using the sol-gel method.

2. Experimental

2.1. *Synthesis of pure and C-doped TiO_2 NPs*

The chemicals titanium butoxide [$Ti(OC_4H_9)_4$] (Aldrich, 98 %) and nitric acid (HNO_3) (Aldrich, 70 %), glucose ($C_6H_{12}O_6$) (Aldrich, 99 %) and ethanol (C_2H_5OH) (Merck, 99 %) were used for the synthesis of carbon -doped TiO_2 nanoparticles.

C-doped TiO_2 nanoparticles for different dopant concentrations (1 %, 2 %, 3 % and 4 %) were synthesized using glucose ($C_6H_{12}O_6$) as a dopant precursor. Graphical representation of mechanism of photocatalysis and method of preparation of C-doped TiO_2 nanoparticles with different concentration by Sol Gel method is shown in Fig. 1. Solution A is prepared by mixing 40 mL of titanium butoxide [$Ti(OC_4H_9)_4$] with 40 mL ethanol (C_2H_5OH). This solution is stirred continuously for one hour at room temperature. Solution B is prepared by mixing glucose (dopant precursor) with 5 mL deionized water, 40 mL ethanol and 0.5 mL nitric acid (HNO_3). Under magnetic stirring for one hour, Solution B is added dropwise into the solution A. The homogeneity of the solution is improved by stirring the solutions for one hour at room temperature. To form the gel the solution was sustained at room temperature for 48 h and then heating at 100 °C for 3 h to remove the excess solvent. The resultant powders after grinding by mortar pestle were calcined at 500 °C for 2 h.

Undoped TiO_2 nanoparticles were synthesized by the same process without the addition of dopant precursor (glucose) in solution A.

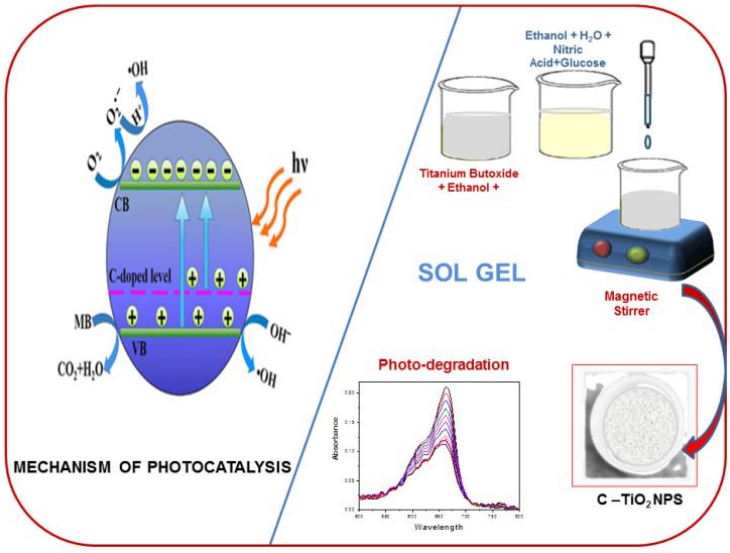

Fig. 1. Graphical representation of mechanism of photocatalysis [26] and method of preparation of C- doped TiO_2 nanoparticles with different concentration by Sol Gel method.

2.2. *Characterization*

X-ray diffractometer (Philips X' Pert PW3040, Netherlands) with Cu Kα radiation source at wavelength (λ) of 1.5405 Å. operated at 40kV and 30 mA is used for XRD measurements. XRD data were collected at 2θ ranging from 20 to 90 degree. Diffraction patterns of all samples were compared with the database of the Joint Committee on Powder Diffraction Standards (JCPDS) files (International Centre for Diffraction Data (ICDD)) to identify their crystalline phase. The surface morphology of all the samples was studied by scanning electron microscope (SEM) (Vega3Tescan, Czech Republic) equipped with energy-dispersive spectroscopy (EDAX) to analyse elemental composition of all the samples and weight and atomic ratio of dopants. In order to confirm the structure of the samples, Raman spectroscopy (Renishaw InVia Micro Raman ,UK) was conducted (Renishaw equipped with a 633 nm laser). The band gap of TiO_2 was determined by measuring UV-VIS diffuse reflectance spectra (Jasco V 760 NIR, Germany) spectrophotometer was used in the range of 200 nm to 800 nm to determine the band gap of TiO_2 samples.

Using methylene blue as the model organic compound, pure TiO_2 and C-doped TiO_2 samples were evaluated for their photocatalytic activity at 30°C. A mixture of 50 ml of aqueous MB (10 mg/L) solution containing 5 mg of prepared photocatalyst was stirred into the glass beaker to conduct the photocatalytic degradation experiment. The equilibrium of adsorption and desorption of the molecules in the suspension was achieved after 30 min of continuous stirring of the suspension. Under constant stirring, the solution was irradiated with a 160 watt mercury vapour lamp placed 10 cm vertically above the beaker. An absorption spectrum was obtained using a spectrophotometer (Equiptronics Eq823) by withdrawing two ml of the solution from the beaker in the cuvette. In order to assess methylene blue's photocatalytic degradation, a plot of its normalized intensity at wavelength 665 nm against exposure time was obtained. The same procedure carried out without addition of catalyst is referred as blank reaction.

3. Results and Discussion

3.1 *X-ray Diffraction*

XRD technique is used for the analysis of the phase identification, purity and crystalline nature of the samples. A comparison of the XRD patterns of pure TiO_2 and C-doped TiO_2 is shown in Fig. 2. The diffraction peaks detected at 2θ of 25.33°,37.9°, 48.03°, 54.3°, 62.7°, 68.4° and 75.02° and 82.7 (JCPDS file no. 21–1272) [28] are resembles to planes (101), (004), (200), (105), (211), (204), (116), (215) and (224) of the anatase phase of TiO_2 (JCPDS Card No. 01-084-1285) [27]. However, some weak additional reflexes have also been linked to the rutile phase as well. The peak at 2θ of 27.60° (JCPDS file no. 21–1276) are attributed to planes (110) of rutile phase (78-2485) [29]. XRD pattern in Fig. 2 shows peaks for anatase phase in all C-doped TiO_2 samples which prove that the

presence of impurity does not affect the crystalline phase. Absence of peaks corresponding to carbon indicates that carbon is doped into TiO_2.

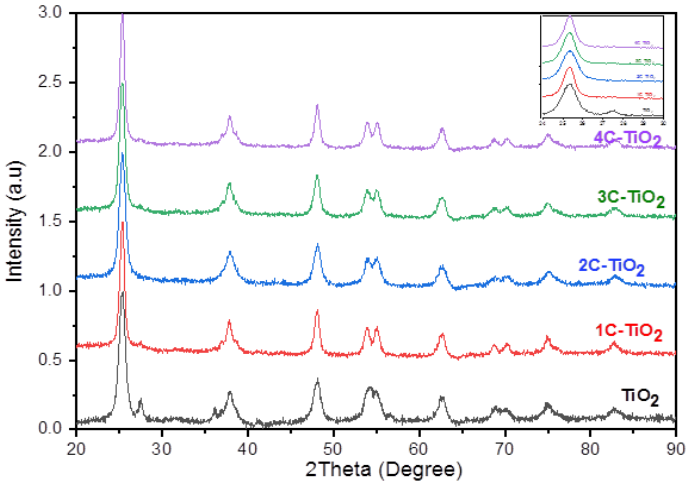

Fig. 2. X-ray diffraction pattern of Pure and C-doped TiO_2 with different C/Ti ratios.

The average crystallite size of the pure TiO_2 and C-doped TiO_2 nanoparticles is computed for the plane (101) (Table 1) using Sherrer's equation [30] $D=0.9\lambda/\beta\cos\theta$ where *D* is the average crystallite size (nm), λ is the wavelength of the X-ray radiation, β is the full width at half maximum intensity, and θ is the diffraction angle. The crystallite size of the prepared samples increased with the dopant concentration in TiO_2 and is in the range of 9.4 to 12.6 nm which is slightly higher than undoped TiO_2 (Table 1) which is also exhibited in earlier studies [27].

The lattice constants a, b and c determined by the equation $1/d^2= (h^2+k^2)/a^2+ l^2/ c^2$ [31] confirmed the tetragonal structure of the crystal (Table 1) The slight variation in interplaner spacing and lattice constants confirms that the Carbon dopant is incorporated into TiO_2 (Table 1)

Table 1: Crystallite size, Anatase Percentage, lattice constants and band gap of pure and C-doped TiO_2

Sample	d spacing (nm)	Crystallite size (nm)	Anatase (%)	Lattice constant	
				a=b(nm)	c(nm)
TiO_2	0.3513	9	83	0.3782	0.9483
1C-TiO_2	0.3515	12.2	100	0.3783	0.9450
2C-TiO_2	0.3511	9.4	100	0.3779	0.9483
3C-TiO_2	0.3514	10.8	100	0.3783	0.9494
4C-TiO_2	0.3512	12.6	100	0.3781	0.9491

3.2 *SEM and EDAX*

Vega3Tescan, a SEM equipped with energy-dispersive spectroscopy (EDAX), was used to obtain the surface morphology of all the samples. In Fig. 3 SEM images are shown for pure TiO_2 and TiO_2 doped with varying carbon dopant concentrations for Carbon doped TiO_2. In all synthesized samples, agglomerated particles developed due to high calcination temperatures and are randomly distributed in each of the samples [32].

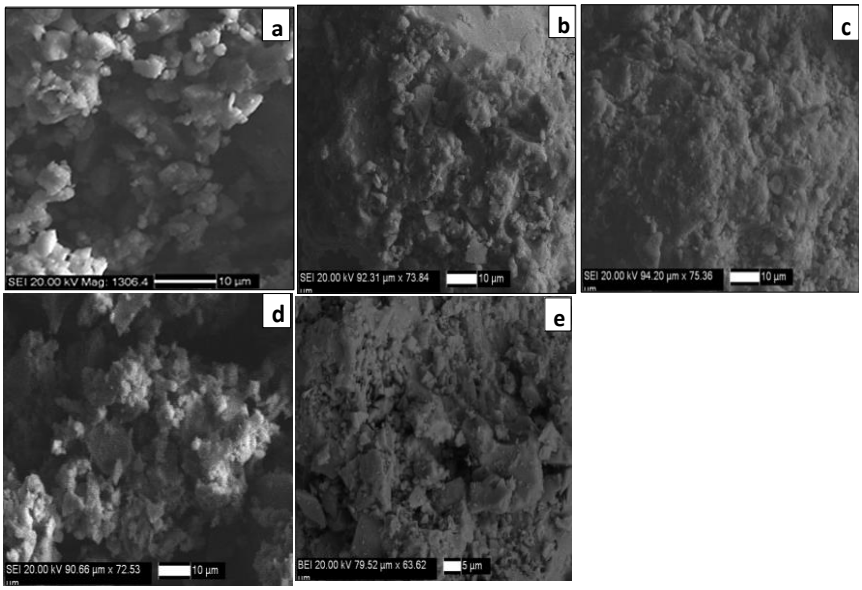

Fig. 3. SEM images of a) TiO_2, b) 1C-TiO_2, c) 2C-TiO_2, d) 3C-TiO_2 and e) 4C-TiO_2.

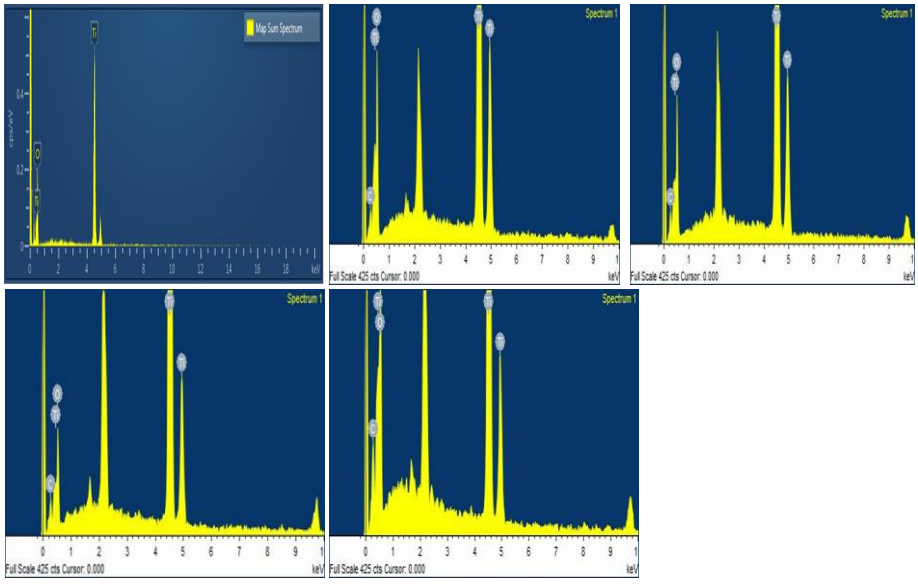

Fig. 4. EDAX spectra of a) TiO_2, b) 1C-TiO_2, c) 2C-TiO_2, d) 3C-TiO_2 and e) 4C-TiO_2.

It was observed that the concentration of Ti was increased with decrease in the concentration of O in TiO_2 lattice with the addition of impurities. It helped to boost the photocatalytic activity of the photocatalyst. No peaks are detected for other components. In EDAX analyses, Au peak have been observed due to the application of a gold coating on the samples before analyzed by SEM and EDAX.

Table 2. Elemental composition and energy bandgap of pure and C-doped TiO_2 with various dopant concentrations.

Sample	Elemental Composition wt%			
	Ti	O	C	Band Gap (eV)
TiO_2	53.94	46.06	-	3.19
1C-TiO_2	57.52	40.11	2.37	3.17
2C-TiO_2	60.27	36.96	2.78	3.12
3C-TiO_2	62.31	33.84	3.86	3.02
4C-TiO_2	62.8	33.2	4.99	2.98

3.3 *Raman spectra*

Raman spectra for pure and C-doped TiO_2 recorded with 633 nm laser, power 0.5 mW and for 100 sec acquisition time are shown in Fig. 5. In Raman spectra of pure TiO_2, the peaks centered at the wavelengths of 144, 196, 396, 516, and 638 cm^{-1} are corresponded to the $E_{g(1)}$, $E_{g(2)}$, $B_{1g(1)}$, $B_{1g(2d)}$, and $E_{g(3)}$ modes of the anatase phase in TiO_2 respectively [33,34]. As carbon content rises, the peaks narrowed, indicating a growth in crystallite size. The peaks for C doped TiO_2 are a bit displaced to the left with increasing dopant concentration, which reveals a slight red shift and demonstrates the existence of impurities or defects in samples. The Raman spectra of the sample might be affected by the interaction of the vibrational modes with contaminants, which is why the peaks are displaced [34].

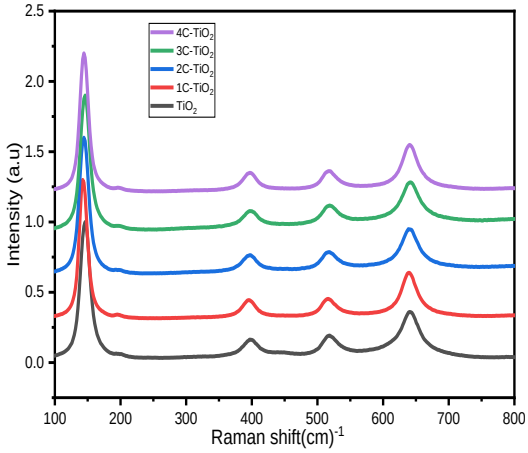

Fig. 5. Raman Spectra of pure and C-doped TiO_2 with different concentrations.

3.4. *UV-vis diffuse reflectance spectra*

Fig. 6 displays the diffuse UV-vis absorption spectra of pure and C-doped TiO_2 nanomaterials with various dopant concentrations. An increase in the dopant concentration has shown increase in the absorbance in the visible spectrum

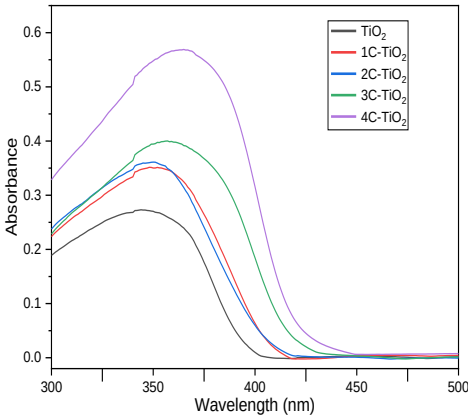

Fig. 6. UV-vis absorption spectra of pure $TiO_2$and C-doped TiO_2 at various C/Ti ratio

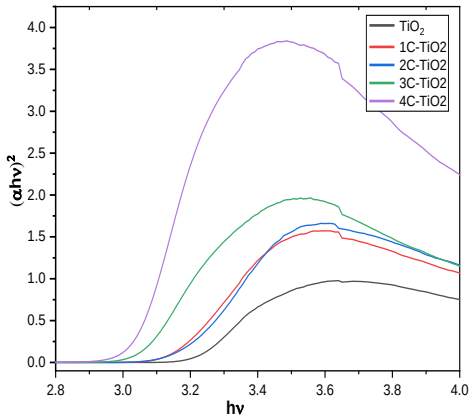

Fig. 7. Tauc plots of pure $TiO_2$and C-doped TiO_2 at various C/Ti ratio

Energy band gap of the prepared samples was estimated by Tauc's formula

$$\alpha h\nu = A(h\nu - E_g)^n$$

where hν is the photon energy, α- is the linear absorption coefficient, A is the proportionality constant and Eg is the bandgap energy and n= 1⁄2 for direct or n = 2 for indirect allowed transition semiconductors [30]. The energy band gap of the samples were derived by taking the intercept of the tangent to the plots of $(\alpha h\nu)^2$ versus photon energy (hν) [12] as shown in Fig. 7. The energy band gap is reduced from 3.19 eV to 2.98 eV with the increase in the amount of impurity as the carbon atoms are incorporated in TiO_2 crystal structure. The substitution of C at O sites in TiO_2 caused the electronic band structure of TiO_2 to be modified by blending the 2p orbitals of C with those of O, resulting in the narrowing of the bandgap [35].

3.5. *Photocatalytic activity*

As a result of the photocatalytic action, a reaction induced by light can be accelerated and enhanced without the photocatalyst being consumed by the reaction itself. As demonstrated by the photodegradation of methylene blue under mercury vapour lamp, C-doped samples were evaluated for the photocatalytic activity and compared with the activity of pure TiO_2 (Fig. 8). The percentage photodegradation rate of Methylene blue dye using pure and C-doped TiO_2 nanoparticles were calculated by the following equation:

$$\text{Photodegradation Rate (\%)} = \frac{Co-Ct}{Co} \times 100\%$$

where Co is the initial concentration and Ct is the concentration of Methylene blue after completion of photocatalytic reaction exposing to visible light [26].

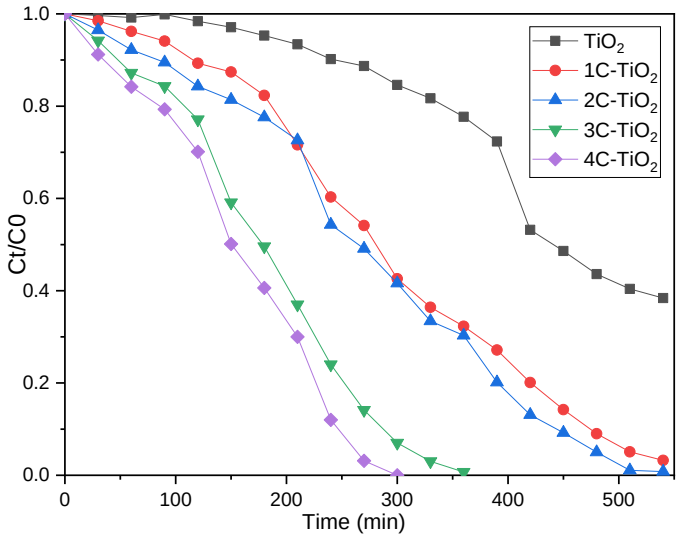

Fig. 8. Photocatalytic degradation of methylene blue in the presence of pure TiO_2 and C-TiO_2 at various dopant concentration under light irradiation.

It is found that pure TiO_2 has the lowest photocatalytic activity having 61 % degradation rate in 540 minutes. The photocatalytic activity of C–doped TiO_2 was enhanced with increasing carbon content in TiO_2 with 96 % and 99 % degradation rate in 540 min for 1C-TiO_2 and 2C-TiO_2. The solution was decolourized with degradation of 100 % for 3C-TiO_2 and 4C-TiO_2 in 360 and 300 minutes respectively. This enhanced photocatalytic activity of C-doped TiO_2 could be due to narrowed band gap derived from the overlapping of C-2p and O-2p states. As a result of the presence of carbon in carbon-doped TiO_2, all the tested samples showed higher photocatalytic activity compared to pure TiO_2 due to the fact that carbon serves as an electron scavenger.

4. Conclusion

Pure and carbon doped TiO_2 nanoparticles with various dopant concentrations were synthesized by sol gel method using titanium butoxide as a precursor for titanium dioxide and glucose as a source of carbon. The effect of doping concentrations on structural, morphological, optical properties were studied by SEM-EDAX analysis, Raman spectroscopy, XRD, and DRS. The XRD revealed that all the samples had good crystallisation with maximum anatase phase structures and with the particle size of about 9 nm to 12.6 nm. The absorption edge of the samples shifts towards higher wavelengths with increasing dopant concentration to decrease the energy band gap from 3.19 eV of

pure TiO_2 to 2.98 eV. The photocatalytic activity of the C-doped TiO_2 samples was investigated by degrading an organic pollutant Methylene blue under Mercury lamp by measuring the normalised intensity of the absorption band at 665 nm which showed that C-doped TiO_2 sample has highest photocatlytic activity.

References

1. A. Piatkow'ska, M. Janus, K. Szyman'ski, and S. Mozia, Catalysts **11**, 144 (2021). https://doi.org/10.3390/catal11010144
2. A. A. Azzaz, J. S. Hamed, N. B. H. El Jery, A. Khezami L., A. A. Assadi, and A. Amrane, Catalysts **11**, 855 (2021). https://doi.org/10.3390/catal11070855
3. P. S. Basavarajappa, S. B. Patil, N. Ganganagappa, K. R. Reddy, A. V. Raghu, and C. V. Reddy, Int. J. Hydrogen Energy **45**, 13 (2020). https://doi.org/10.1016/j.ijhydene.2019.07.241
4. Y. Park, W. Kim, H. Park, T. Tachikawa, T. Majima, and W. Choi, Appl. Catal. B Environ. **91**, **1-2**, 357 (2009). https://doi.org/10.1016/j.apcatb.2009.06.001
5. S. Modanlu and A. Shafiekhani, Sci. Rep. **9**, ID 16648 (2019). https://doi.org/10.1038/s41598-019-53189-z
6. P. Nyamukamba, L. Tichagwa, S. Mamphweli, and L. Petrik, Int. J. Photoenergy **2017**, ID 3079276 (2017). https://doi.org/10.1155/2017/3079276
7. A. Fujishima, X. Zhang, and D. A. Tryk, Surf. Sci. Rep. **63**, 12 (2008). https://doi.org/10.1016/j.surfrep.2008.10.001
8. M. A. Behnajady, B. Alizade, and N. Modirshahla, Photochem. Photobiol. **87**, 6 (2011). https://doi.org/10.1111/j.1751-1097.2011.01002.x
9. S. G. Kumar and L. G. Devi, J. Phys. Chem. A **115**, 46 (2011). https://doi.org/10.1021/jp204364a
10. M. Sun, H. Liu, Z. Sun, and W. Li, J. Environ. Chem. Eng. **8**, 5 (2020).
11. N. Umezawa and J. Ye, Phys. Chem. Chem. Phys. 14, 17 (2012). https://doi.org/10.1039/c2cp24010f
12. P. Junlabhut, C. Wattanawikkam, W. Mekprasart, and W. Pecharapa, J. Nanosci. Nanotechnol. **18,** 7302 (2018). https://doi.org/10.1166/jnn.2018.15717
13. M. Sadia , R. Naz , J. Khan , M. Zahoor, R. Ullah , R. Khan , S. Naz , H. S. Almoallim, and S. A. Alharbi, J. King Saud Univ. - Sci. **33**, ID 101322 (2021). https://doi.org/10.1016/j.jksus.2020.101312
14. A. N. Banerjee, N. Hamnabard, and S. W. Joo, Ceram. Int. **42**,10, (2016). https://doi.org/10.1016/j.ceramint.2016.04.128
15. C. G. Wu, C. C. Chao, and F. T. Kuo, Catal. Today **97,** 103 (2004). https://doi.org/10.1016/j.cattod.2004.04.055
16. I. Marić, M. Gotić, T. Jurkin, L. Mikac, É. Tronc, and M. Ivanda, Croat. Chem. Acta **91**, 577 (2018). https://doi.org/10.5562/cca3441
17. F. Zhang, X.Wang , H. Liu , C. Liu , Y. Wan , Y. Long and Z. Cai, Appl. Sci. **9**, ID 2489 (2019). https://doi.org/10.3390/app9122489
18. S. N. A. Sulaiman, M. Zaky Noh, N. Nadia Adnan, N. Bidin, and S. N. Ab Razak, J. Phys. Conf. Ser. **1027**, ID 012006 (2018). https://doi.org/10.1088/1742-6596/1027/1/012006
19. Y. N. Tan, C. L. Wong, and A. R. Mohamed, ISRN Mater. Sci. **2011**, ID 261219 (2011). https://doi.org/10.5402/2011/261219
20. P. Nyamukamba, L. Tichagwa, and C. Greyling, Mater. Sci. Forum **712**, 49 (2012). https://doi.org/10.4028/www.scientific.net/MSF.712.49
21. T. Ohno, Water Sci. Technol. **49**, 159 (2004). https://doi.org/10.2166/wst.2004.0250
22. T. T. Khan, G. A. K. M. R. Bari, H. -J. Kang, T. -G. Lee, J. -W. Park, H. J. Hwang, S. M. Hossain , J. S. Mun, N. Suzuki, A. Fujishima , J. -H. Kim , H. K. Shon, and Y. -S. Jun, Catalysts **11**, 109 (2021). https://doi.org/10.3390/catal11010109

23. S. A. Ansari, M. M. Khan, M. O. Ansari, and M. H. Cho, New J. Chem. **40**, 3000 (2016). https://doi.org/10.1039/C5NJ03478G
24. T. A. Vu, C. D. Dao, T. T. T. Hoang, G. H. Le, K. T. Nguyen, P. T. Dang, H. T. K. Tran, T. V. Nguyen, Int. J. Nanotechnol. **10**, 3 (2013).
25. C. Belver, J. Bedia, A. Gómez-Avilés, M. Peñas-Garzón, and J. J. Rodriguez, in Nanoscale Materials in Water Purification (Elsevier Inc., 2019) pp. 581–651. https://doi.org/10.1016/B978-0-12-813926-4.00028-8
26. J. Zhang, G. -F. Huang, D. Li, B. -X. Zhou, A. Pan, and W. -Q. Huang, Appl. Phys. A Mater. Sci. Process.**122,** ID 994 (2016). https://doi.org/10.1007/s00339-016-0522-9
27. N. U. M. Nor and N. A. S. Amin, J. CO_2 Util. **33**, 372 (2019). https://doi.org/10.1016/j.jcou.2019.07.002
28. S. K. Kuriechen and S. Murugesan, Water. Air. Soil Pollut. **224**, ID 1671 (2013), https://doi.org/10.1007/s11270-013-1671-5
29. H. P. Shivaraju, G. Midhun, K. M. A. Kumar, S. Pallavi, N. Pallavi, and S. Behzad, Appl. Water Sci. **7**, 3937 (2017). https://doi.org/10.1007/s13201-017-0546-0
30. N. Nithya. S. Gopi, G. Bhoopati, Inorg. Organomet. Polym. Mater. **31**, 4594 (2021). https://doi.org/10.1007/s10904-021-02076-0
31. A. E. Pirbazari, P. Monazzam, and B. F. Kisomi, Desalin. Water Treat. **63** (2017).
32. A. K. Singh and U. T. Nakatele, J. Nanoparticles **2013**, ID 310809 (2013). https://doi.org/10.1155/2013/310809
33. R. Jaiswal, J. Bharambe, N. Patel, A. Dashora, D. C. Kothari, and A. Miotello, Appl. Catal. B Environ. **168–169**, 333 (2015). https://doi.org/10.1016/j.apcatb.2014.12.053
34. X. Chen and S. S. Mao, Chem. Rev. **107**, 2891 (2007). https://doi.org/10.1021/cr0500535
35. A. Y. and H. Z. Fei Huang, in Semiconductor Photocatalysis - Materials, Mechanisms and Applications blue, ed. W. Cao et al. (CBS Publishers & Distributors Pvt. Ltd. Croatia: 2016) pp. 31–80. https://doi.org/10.5772/63234